Available online at www.sciencedirect.com
SCIENCE DIRECT®
Journal of Molecular Catalysis A: Chemical 211 (2004) 165–177
JOURNAL OF MOLECULAR CATALYSIS A: CHEMICAL
www.elsevier.com/locate/molcata

A comparative study on the catalytic activity of Zn and Fe containing Al-MCM-41 molecular sieves on *t*-butylation of phenol

R. Savidha*, A. Pandurangan, M. Palanichamy, V. Murugesan

Department of Chemistry, Anna University, Chennai 600025, India

Received 9 June 2003; received in revised form 6 October 2003; accepted 7 October 2003

Abstract

Mesoporous Al-MCM-41, Zn– and Fe–Al-MCM-41 molecular sieves with different metal contents were synthesised hydrothermally. The hexagonal structure of synthesised materials was confirmed by low angle XRD. The textural properties were measured by nitrogen adsorption studies. ^{27}Al MAS NMR was used to study the co-ordination environment of aluminium. Diffuse reflectance spectra (DRS) and electron paramagnetic resonance (EPR) studies also confirm the co-ordination environment of Fe in Fe–Al-MCM-41 framework. The acidity of the catalysts was measured by TPD of NH_3 and pyridine adsorbed FT-IR spectroscopy. *t*-Butylation of phenol with *t*-butyl acetate (TBA), a new alkylating agent was carried out in vapour phase over the mesoporous materials. For comparison purpose Zn and Fe ion exchanged Al-MCM-41 were also used. The effect of feed molar ratio, phenol space velocity and reaction temperature were studied and the results are discussed. Conditions were optimised to get better phenol conversion and 4-*t*-butyl phenol (4-TBP) selectivity.

Keywords: Al-MCM-41; Zn–Al-MCM-41; Fe–Al-MCM-41 molecular sieves; *t*-Butyl acetate; *t*-Butylation; 4-*t*-Butyl phenol

1. Introduction

The reaction of *t*-butylation of phenol, an industrially important reaction, have been studied extensively owing to the immense application of *t*-butylated phenolic compounds in the production of antioxidants, phenolic resins, ultraviolet adsorbers, heat stabilisers of polymeric materials, lube additives and substituted triaryl phosphates [1,2]. It is a Friedel–Crafts class of reaction and is generally carried out over strong acids, which are highly toxic and corrosive. Supporting the acid catalysts on zeolite can solve many of these problems. Few reports are available on the *t*-butylation of phenol over zeolites like HY [3], Hβ [4] and activated clay [5] in gas or liquid phase. It is observed that the weakly acidic zeolites like Y [6] led to O-alkylated products while the strongly acidic zeolites like β [7] resulted in C-alkylated products. Zhang et al. [4] studied the *t*-butylation of phenol with *t*-butanol over zeolite Hβ and found that strong acid sites are helpful for the formation of 2,4-DTBP and medium acid sites are advantageous to produce *p*-isomer (*p*-TBP), while weak acid sites are effective to produce *o*-isomers. The methylation of phenol with methanol over zeolites and metal oxides in gas phase reveals that the acidic and basic properties of the catalysts play an important role in product selectivity: a change in acidity causes a change in alkylation selectivity [8–10]. Although the zeolites are advantageous, the use of zeolites has been restricted in recent years owing to the limitations: the greater sensitivity to deactivation by irreversible adsorption or steric blockage of heavy secondary products and the impossibility of using their microporosity for the synthesis of bulky molecules. The mesoporous MCM-41 molecular sieves, a member of M41S family possesses large internal surface area (normally over 1000 m^2/g), massive accessible pore volume (normally over 0.8 ml/g), one dimensional pore geometry and hydrophobic surface property has attracted much research attention owing to their potential application as catalysts, ion exchangers, molecular clusters, catalyst support and adsorbent [11,12]. Because of the absence of active sites in their matrices, pure silicious mesoporous molecular sieves are of limited use as catalysts. The incorporation of transition metals such as Al, Fe, Zn and Mn [13–19] in the silica framework has been implemented in order to increase the acidity and catalytic activity of the mesoporous silica molecular sieves. Sakthivel et al.

* Corresponding author. Tel.: +91-44-22-354965; fax: +91-44-22-350397.
E-mail address: savidharam@yahoo.com (R. Savidha).

1381-1169/$ – see front matter © 2003 Elsevier B.V. All rights reserved.
doi:10.1016/j.molcata.2003.10.022

[20] carried out *t*-butylation of phenol over H–Al-MCM-41 and observed higher substrate conversion and *p*-selectivity than that over zeolites and SAPOs and accounted in terms of moderate-to-strong acidity, large surface area and mesoporous nature of the H–Al-MCM-41. He et al. [21] reported that Fe-MCM-41 molecular sieves were very active in benzylation of benzene with 100% monoalkylation selectivity and better stability.

In conventional methods, isobutene and *t*-butyl alcohol has been used as the alkylating agent for phenol. These reagents possess some demerits as the former could deactivate the catalyst by yielding polybutenes (oligomerisation) [4], and the later, *t*-butyl alcohol, although could discourage the coke formation, would get aggregated near Brønsted acid sites through hydrogen bonding thereby suppressing dissociation. Changing over to *t*-butyl acetate (TBA) it has many advantageous over the conventional reagents, as it could get better adsorbed on the Brønsted acid sites. It may be due to the easy availability of free active sites for adsorption namely the carbonyl group of TBA, compared to the sterically crowded alcoholic OH in *t*-butyl alcohol. Isopropyl acetate has been proved to be a better phenol alkylating agent in our previous study [22].

In the present study, MCM-41 materials containing zinc and iron have been synthesised by hydrothermal crystallisation process. The structural and textural properties of the synthesised materials have been characterised by employing various physicochemical techniques. The feasibility of phenol alkylation with *t*-butyl acetate over these catalysts and the important factors affecting the conversion and selectivity of the reaction such as reaction temperature, space velocity, mole ratio of phenol to TBA and acidity were studied and the results are discussed.

2. Experimental

2.1. Synthesis of catalytic materials

Al-MCM-41 (Si/Al = 100 and 50) samples were synthesised hydrothermally using a gel composition of SiO_2:xAl_2O_3:0.2CTAB:0.89H_2SO_4:120H_2O (*x* varies with Si/Al ratio). Sodium metasilicate (E-Merck) and aluminium sulphate (E-Merck) were used as the sources for silicon and aluminium, respectively. Cetyl trimethyl ammonium bromide (CTAB) (E-Merck) was used as the structure directing agent. In a typical synthesis, 10.6 g of sodium metasilicate in water was combined with appropriate amount of aluminium sulphate in distilled water and the pH of the solution was adjusted to 10.5 with constant stirring to form a gel. After 30 min, an aqueous solution of CTAB was added and the mixture was stirred for 1 h at room temperature. The suspension was then transferred into a 300 ml stainless steel autoclave, sealed and placed in a hot air oven at 160 °C for 48 h. After cooling to room temperature, the product formed was filtered, washed with deionised water and dried. Using zinc sulphate (E-Merck) and ferric nitrate (E-Merck) as sources for Zn and Fe, respectively, Zn– and Fe–Al-MCM-41 with Si/M (M = Zn and Fe) ratio 100 and 50 were also synthesised by adopting the same procedure. In both Zn– and Fe–Al-MCM-41 catalysts, the Si/Al ratio was kept as 100. The dried materials were calcined at 550 °C for 6 h in nitrogen atmosphere. The calcined materials were converted into H-form by repeated ion exchange with aqueous 1 M NH_4Cl solution followed by calcination at 550 °C for 6 h. The ion exchanged Zn– and Fe–Al-MCM-41 molecular sieves were prepared by exchanging Zn^{2+} and Fe^{3+} ions in H-form of Al-MCM-41 molecular sieves by using 0.2 M aqueous $Zn(NO_3)_2$ and $Fe(NO_3)_3$ solutions at pH 1.7 and ambient temperature for 24 h. The resulting materials were filtered, dried at 110 °C and calcined at 550 °C in air.

2.2. Characterisation

The purity and structure of the calcined Al-MCM-41 (50), Zn– and Fe–Al-MCM-41 (50) materials were analysed by low angle X-ray powder diffractions on a Philips PW1050 diffractrometer equipped with liquid nitrogen-cooled germanium solid-state detector using Cu Kα radiation. The samples were scanned from 1 to 10° (2θ) in steps of 0.02 with the counting time of 5 s at each point. The surface area measurements of all the catalyst samples were carried out in nitrogen adsorption at 77 K in an ASAP-2010 volumetric adsorption analyser manufactured by Micromeritics Corporation (Norcross, Ga). Before the nitrogen adsorption–desorption measurements, each sample was degassed at 623 K at 1.333×10^{-3} N/m^2 overnight. The specific areas of the samples were determined from the linear part of the BET plots. The pore size distribution was calculated from the nitrogen adsorption–desorption isotherms using the BJH algorithm (ASAP201 built in software from Micromeritics). Chemical analysis was performed with an ICP-AES Labtum plasma 8440 instrument. The content of SiO_2 and Al_2O_3 was determined after dissolution with HF and borax, respectively.

The size and morphology of Al-MCM-41 (50), Zn– and Fe–Al-MCM-41 (50) samples were examined by scanning electron microscopy using JEOL 640 instrument. Samples were gold coated using an instrumental scientific instruments PS-2 coating unit. The SEM pictures are developed using thin photographic paper. Solid-state ^{27}Al MAS NMR measurements for Al-MCM-41 (50), Zn– and Fe–Al-MCM-41 (50) catalysts were performed on a MSL 400 spectrometer equipped with a magic angle spinning (MAS) unit to analyse the Al environment. The ^{27}Al chemical shifts were reported in relation to the liquid solution of aluminium nitrate.

The co-ordination environment of Fe in Fe–Al-MCM-41 samples was examined by diffuse reflectance UV-Vis spectroscopy. The spectra were recorded in Shimadzu (UV-Vis spectrophotometer model 2101 PC) in the wavelength range of 200–600 nm. The co-ordination environment of Fe in Fe–Al-MCM-41 (50 and 100) samples was further confirmed by EPR analysis recorded on a JEOL EPR

spectrometer (JES-RE1XM) operating in the *X*-band region. DPPH ($g = 2.0037$) was used as a reference to mark the *g*-value.

2.3. Acidity measurements

The acidity of Al-MCM-41 and substituted Al-MCM-41 materials was analysed by both TPD of NH_3 by TGA method as well as pyridine adsorption followed by FT-TR spectroscopy. About 1.0 g of the sample was packed in a quartz tube and the initial flushing was carried out with dry nitrogen for 3 h. Then the system was evacuated (1.999×10^{-3} N/m^2) at 550 °C for 5 h and cooled to room temperature. Ammonia adsorption was carried out by passing the ammonia vapours over the catalyst bed. After adsorption, the system was evacuated to remove the physisorbed ammonia and again ammonia was passed through the system. The adsorption and evacuation processes were repeated five times for saturating the molecular sieves. The extent of ammonia adsorbed over each catalyst was measured by TGA in a TA 3000 Mettler system. Nitrogen as purge gas was passed during desorption of ammonia. The TGA study was conducted at a heating rate of 10 °C/min up to 600 °C.

Finely ground catalyst sample (10–15 mg) was pressed (for 2 min at 10 t/cm^2 pressure under vacuo) into a self-supporting wafer. The wafers were calcined under vacuo (133.322×10^{-3} N/m^2) at 500 °C for 2 h, followed by exposure to pyridine vapour at ambient temperature for 1 h to allow the pyridine to permeate the samples. The thin wafer was placed in the FT-IR cell and the spectrum was recorded in absorbance mode on a Nicolet 800 (AVATAR) FT-IR spectrometer, fully controlled by the OMNIC software, and an all-glass high-vacuum system. The difference between the spectra of pyridine adsorbed on the samples and that of the reference was obtained by subtraction.

2.4. Catalytic studies

The catalytic activity measurements were carried out in a fixed bed continuous down flow quartz reactor under atmospheric pressure in the temperature range of 250–400 °C in steps of 50 °C. The reactor packed with 1.0 g of catalyst was placed in a tubular furnace. The catalyst was activated in nitrogen atmosphere for 1 h followed by air for 5 h at 550 °C and then cooled under a nitrogen stream to the desired reaction temperature. The feed mixture was injected using a syringe infusion pump at a predetermined flow rate. The reaction was carried out by changing the reactant feed ratio, space velocity and reaction temperature. The products were collected in a cold trap for a time interval of 1 h. The products were analysed by gas chromatography (Hewlett-Packard 5890A) equipped with flame ionisation detector and SE-30 column. The identification of products was also done by GC–MS (Perkin-Elmer Elite series PE-5, capillary column, 30 m × 0.25 mm × 1 μm). The material balance calculation shows that more than 95% of the reactants were recovered as products. No significant phenol conversion is observed when the reaction is carried out without catalyst indicating that there is no thermal effect on conversion.

3. Results and discussion

3.1. Characterisation

3.1.1. Low angle XRD analysis

The low angle XRD patterns of calcined Al-MCM-41 (50), Zn– and Fe–Al-MCM-41 (50) samples are shown in Fig. 1. It can be observed that all the above materials exhibit a strong peak in the 2θ range 1.8–2.2° due to (1 0 0) plane reflection lines and small peaks due to higher order 1 1 0, 2 0 0 and 2 1 0 plane reflections indicating the formation of a well-ordered mesoporous materials. These peaks are generally indexed according to the hexagonal regularity of MCM-41. Let us note that the XRD patterns obtained are found to be in good agreement with a previous report for similar materials [23]. Further, the appearance of the above peaks in Zn– and Fe–Al-MCM-41 (50) catalysts suggests that the hexagonal array of mesopores in MCM-41 was sustained after the incorporation of Zn and Fe in the framework. The reduction in peak intensity and broadening of 1 0 0 peak of Zn– and Fe–Al-MCM-41 samples are the indications of the slight reduction of hexagonal symmetry of MCM-41 due to Zn and Fe incorporation. In the case of substituted Al-MCM-41, the *d*-spacing and hence the

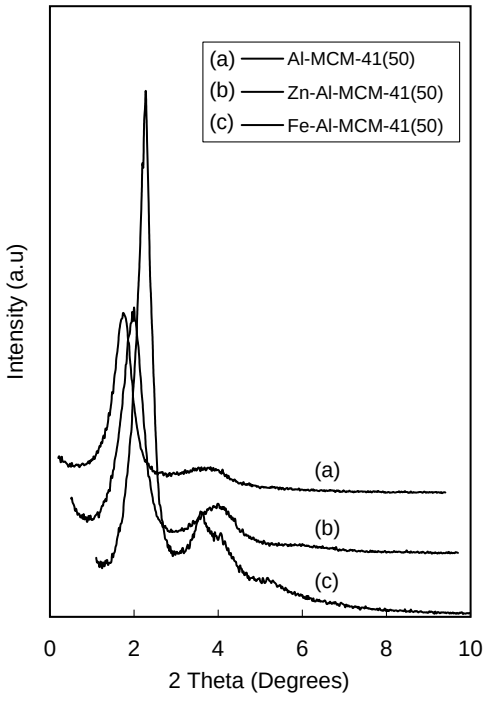

Fig. 1. Low angle XRD patterns of (a) Al-MCM-41 (50), (b) Zn–Al-MCM-41 (50) and (c) Fe–Al-MCM-41 (50) catalysts.

unit cell parameter (a_0) calculated from $2d(1\,0\,0)/\sqrt{3}$ is found to be large compared with that of pure Al-MCM-41. The value of *d*-spacing for Al-MCM-41 (50) is 38.4 Å and that of Zn– and Fe–Al-MCM-41 (50) is found to be as 44.1 and 46.5 Å, respectively. The enlargement in the unit cell parameter of the substituted materials is expected, since the incorporation of metal cations with ionic radius larger than Si^{4+} or Al^{3+} leads to larger M–O bond distance. The ionic radius of Zn^{2+} and Fe^{3+} (74 pm) is larger than that of Si^{4+} (40 pm) or Al^{3+} (53 pm), the increase in the *d*-spacing is the indication of the incorporation of Zn^{2+} and Fe^{3+} ions into the Al-MCM-41 framework.

3.1.2. Nitrogen adsorption studies

The nitrogen adsorption isotherm was carried out over the above catalysts and the typical isotherm for catalysts Al-MCM-41 (50), Zn– and Fe–Al-MCM-41 (50) is presented in Fig. 2a–c, respectively. It is observed that there are three different well-defined stages in the isotherms. The initial increase in nitrogen uptake at low P/P_0 may be due to monolayer–multilayer adsorption on the pore walls, a sharp steep increase at intermediate P/P_0 may indicate the capillary condensation in the mesopores and a plateau portion at higher P/P_0 associated with multilayer adsorption on the external surface of the materials. All the catalysts show a characteristic step around $P/P_0 \approx 0.4$ indicating the mesoporous nature of the materials [24]. The sharpness and height of the capillary condensation step are the indications of pore size uniformity. Deviations from sharp and well-defined pore filling step are the indication of increase in pore size heterogeneity. The Al-MCM-41 samples exhibit isotherm with well-developed step in the relative pressure range ≈ 0.42, characteristic of capillary condensation into uniform mesopores. The incorporation of Zn and Fe in the Al-MCM-41 framework is found to lower the P/P_0 for capillary condensation step, indicating the shift in pore size to higher value due to Zn and Fe incorporation. The pore diameter and pore volume is found to decrease with increasing metal (Al, Zn and Fe) incorporation over all the catalysts. Also, all the samples have high BET surface area (929–844 m^2/g), which is characteristic of mesoporous materials. Table 1 shows the detailed physicochemical characteristics of all the catalytic materials.

3.1.3. Scanning electron microscopy

The size and morphology of Al-MCM-41 (50), Zn–Al-MCM-41 (50) and Fe–Al-MCM-41 (50) were investigated by scanning electron microscopy. The SEM pictures of these catalysts are presented in Fig. 3a–c. The samples do not have well-defined hexagonal structure. Further, aggregates without regular shapes are observed in agreement with previous reports [25] for metal incorporated materials, indicating a slight reduction in hexagonal symmetry of MCM-41 due to metal incorporation.

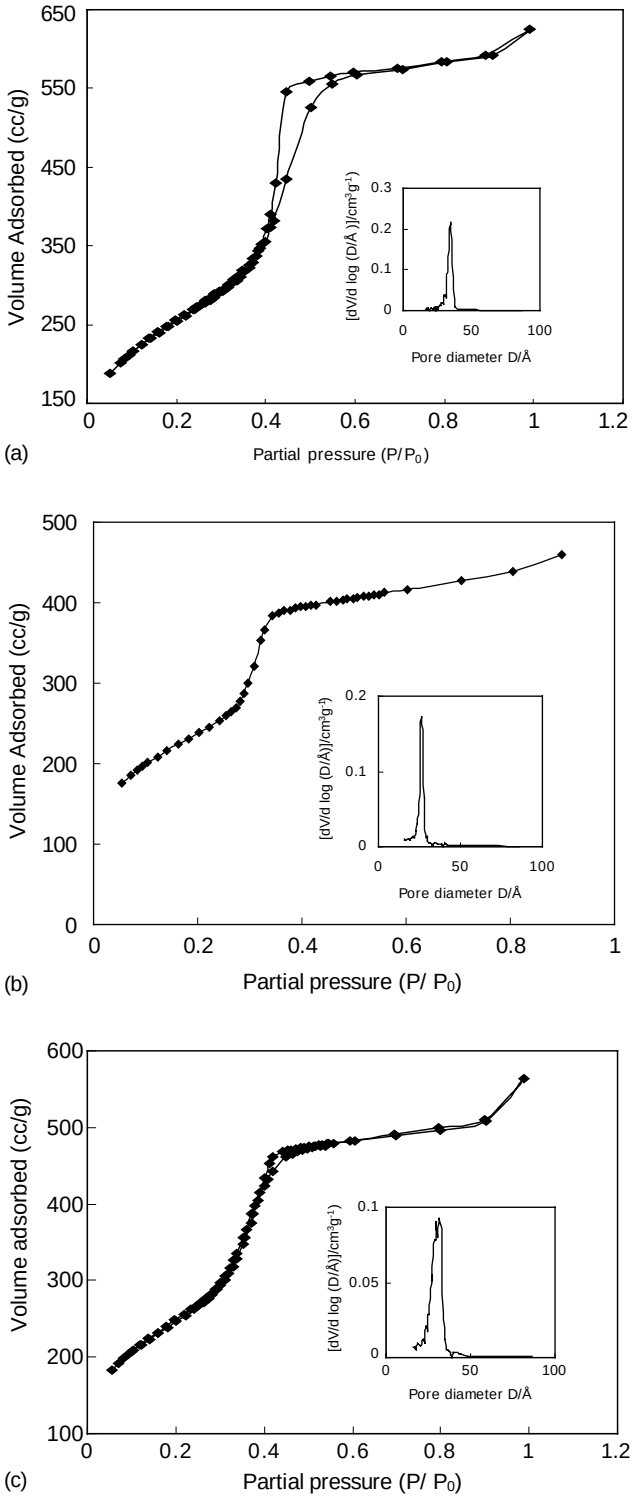

Fig. 2. Nitrogen adsorption isotherm of (a) Al–MCM-41 (50), (b) Zn–Al-MCM-41 (50) and (c) Fe–Al-MCM-41 (50) catalysts.

3.1.4. ^{27}Al MAS NMR

The incorporation of Al into the framework of Al-MCM-41 (50), Zn– and Fe–Al-MCM-41 (50) samples was analysed by ^{27}Al MAS NMR spectroscopy and the spectra of the as-synthesised and calcined form of these samples are

Table 1
Physicochemical characteristics of pure and Zn and Fe incorporated Al-MCM-41 catalysts

Catalyst	Si/M ratio		*d*-Spacing (Å)	BET surface area (m^2/g)	Pore diameter (Å)	Pore volume (cm^3/g)	TPD of NH_3		Total acidity (mmole/g)
	Initial gel	Calcined					LT-peak	HT-peak	
Al-MCM-41	100	107	36.5	929	34.7	0.99	0.175	0.120	0.295
Al-MCM-41	50	52	38.4	893	33.9	0.93	0.210	0.127	0.337
Zn–Al-MCM-41	100	102	43.2	878	32.1	0.90	0.277	0.148	0.425
Zn–Al-MCM-41	50	56	44.1	864	31.4	0.87	0.285	0.162	0.447
Fe–Al-MCM-41	100	98.3	45.5	853	30.9	0.88	0.282	0.157	0.439
Fe–Al-MCM-41	50	61.5	46.5	844	30.1	0.83	0.310	0.185	0.495

presented in Fig. 4A and B, respectively. The spectra of the as-synthesised and calcined samples show a sharp resonance peak from tetrahedrally coordinated aluminium at $\delta = 53.2$ and 53.7 ppm, respectively, indicating that aluminium is incorporated into the framework [26]. A peak at 0 ppm corresponding to octahedral aluminium species is not observed in as-synthesised samples. But in the case of calcined samples, a broad low intensity peak at $\delta = 0.6$ ppm indicating the presence of octahedral aluminium. The appearance of octahedral aluminium in calcined samples indicates that during the course of calcination, some aluminium species are removed from the framework. The ^{27}Al signals are found to be broader than the signals generally observed for zeolitic aluminium, presumably due to greater distortions in the tetrahedral environment [27].

3.1.5. DRS

The diffuse reflectance UV-Vis spectra were recorded for calcined Fe–Al-MCM-41 catalysts in order to study the co-ordination environment of Fe and the spectra are shown in Fig. 5. A broad peak around 275 nm, which is similar to that of ferrisilicate containing tetrahedrally co-ordinated iron species was observed over both Fe–Al-MCM-41 catalysts. This band could be assigned to the dπ–pπ charge transfer between the Fe and O atoms in the framework of Fe–O–Si in the zeolite [28]. A small peak around 215 nm may be due to iron in octahedral co-ordination. Also, the as-synthesised samples exhibited white colour, suggesting that no bulk iron oxide existed and all the iron cations were probably incorporated inside the framework after the hydrothermal synthesis. After calcinations the samples become off-white in colour, possibly suggesting the presence of the extra framework iron.

3.1.6. EPR

The co-ordination environment of Fe is further analysed by EPR spectroscopy. The EPR spectrum of calcined Fe–Al-MCM-41 catalysts is shown in Fig. 6. Two signals at $g = 2.0$ and 4.25, were mainly detected. The signal at $g = 4.25$ could be attributed to Fe(III) ion in tetrahedral co-ordination with strong rhombic distortion [29]. The small shoulder at $g = 2.0$ can be attributed to Fe(III) in octahedral co-ordination [30,31].

3.1.7. Acidity measurements

3.1.7.1. TPD of ammonia. The total acidity of all the catalytic materials was measured by TPD of ammonia by TGA method. The desorption temperature and amount of ammonia desorbed are considered as indexes of acid strength and total number of acid sites, respectively. The amounts of ammonia desorbed and desorption temperature of all the catalytic materials are presented in Table 1. It is observed that two major weight losses occurred over all the catalysts at lower and higher temperature ranges, which may be due to the desorption of ammonia adsorbed on weak and strong acid sites, respectively. The first and second weight losses occurred between 200–225 and 385–420 °C, respectively, for all the catalytic systems. No significant change in desorption temperature is observed due to Zn and Fe incorporation in Al-MCM-41. However the amount of ammonia desorbed both in the lower and the higher temperature ranges are found to increase on Zn and Fe incorporation and with increasing metal (Zn or Fe) content. Zn– and Fe–Al-MCM-41 (50) catalysts show the total acidity of 0.447 and 0.495 mmole/g, respectively, which are slightly higher than that of catalyst A1-MCM-41 (50) (0.337 mmole/g).

3.1.7.2. Pyridine adsorbed FT-IR spectroscopy. The FT-IR spectra for Al-MCM-41 (50), Zn– and Fe–Al-MCM-41 (50) containing adsorbed pyridine are presented in Fig. 7. It is observed that all the catalysts have both Brønsted and Lewis acid sites. A typical sharp peak appeared at 1545 cm^{-1} is the indication of pyridine adsorbed on Brønsted acid sites. A small peak at 1455 cm^{-1} and a high intensity peak around 1620 cm^{-1} indicate the pyridine adsorbed on Lewis acid sites. A broad peak appeared around 1500 cm^{-1} is the combination band of Brønsted and Lewis acid sites. It is interesting to note that the intensities of peaks corresponds to Lewis and Brønsted acid sites are found to be higher for Zn– and Fe–Al-MCM-41 (50) catalysts than that of Al-MCM-41 (50), i.e. the incorporation of Zn and Fe in Al-MCM-41 framework increases the number of both Brønsted and Lewis acid sites in accordance with the observation made by TPD of ammonia. The Zn and Fe incorporation in Al-MCM-41 is found to generate additional acidity. The increase in both Lewis

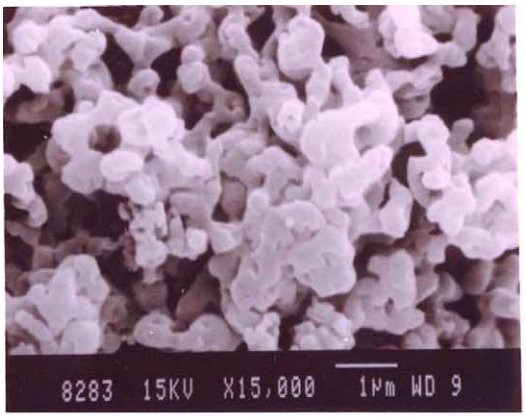

(a)

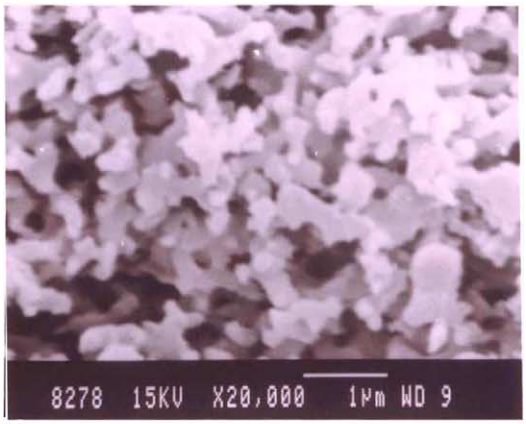

(b)

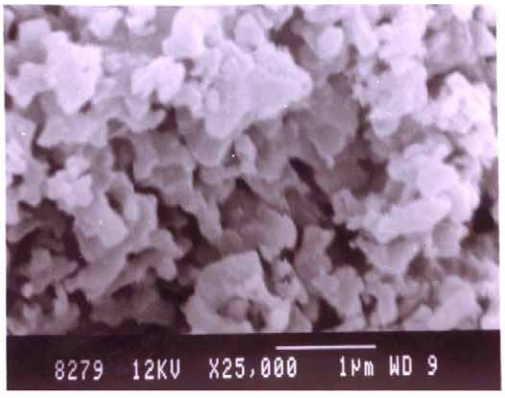

(c)

Fig. 3. SEM pictures of (a) Al-MCM-41 (50), (b) Zn–Al-MCM-41 (50) and (c) Fe–Al-MCM-41 (50) catalysts.

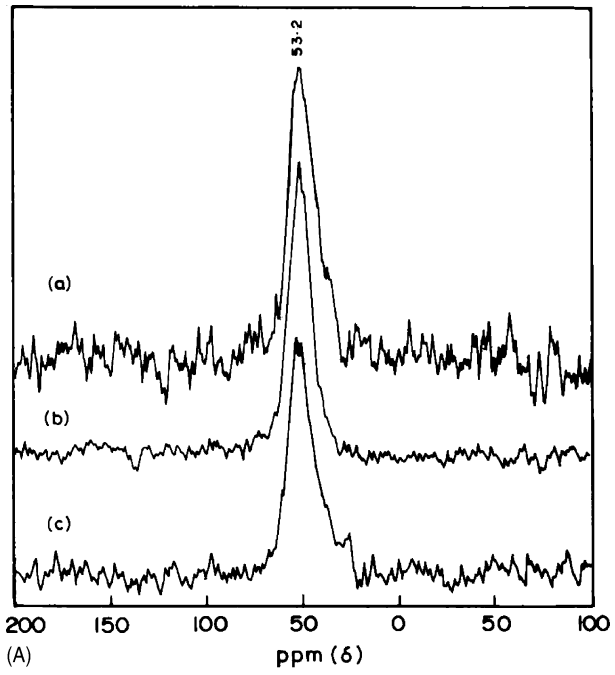

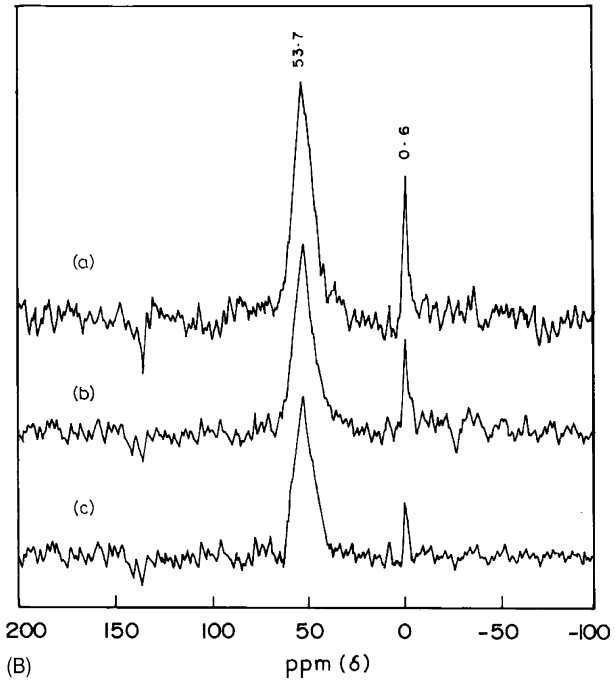

Fig. 4. ^{27}Al MAS NMR spectra of (A) as-synthesised (B) calcined catalysts: (a) Al-MCM-41 (50); (b) Zn–Al-MCM-41 (50); (c) Fe–Al-MCM-41 (50).

and Brønsted acid sites can be related to the presence of appropriately positioned Lewis acid centre with respect to Brønsted acid sites, which may strengthen the acidity of these Brønsted acid sites [32]. Similarly, Zn and Fe, which itself is a Lewis acid, may strengthen the near by Brønsted acid sites (due to Al^{3+} ions), and hence presumed to enhance the over all acidity of Al-MCM-41. The acidity measurements indicate that incorporation of Zn and Fe in tetrahedral co-ordination in Al-MCM-41 structure generates additional acidity due to the strong polarisation of possible $Si–O^{\delta-}\cdots Zn^{\delta+}$ and $Si–O^{\delta-}\cdots Fe^{\delta+}$ linkages. There may be two types of linkages, viz. Si–O···M (M = Zn and Fe) and Si–O···Al which could be due to their different nature and which play an important role in the acid sites distribution of Zn– and Fe–Al-MCM-41 molecular sieves.

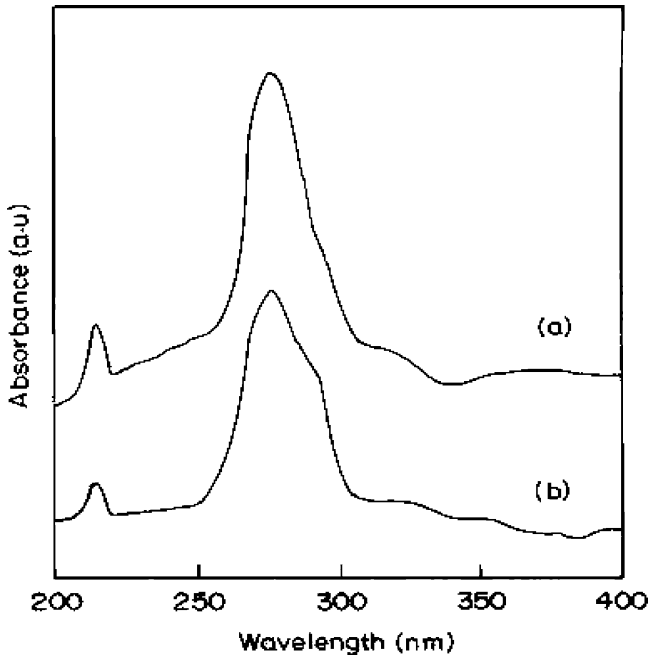

Fig. 5. Diffuse reflectance UV-Vis spectra of Fe–Al-MCM-41 catalysts: (a) Fe–Al-MCM-41 (50); (b) Fe–Al-MCM-41 (100).

3.2. Catalytic studies

t-Butylation of phenol with TBA was carried out over the H-form of Al-MCM-41, Zn– and Fe–Al-MCM-41 catalysts in the temperature range of 250 to 400 °C in steps of 50 °C. The optimised molar ratio of phenol to *t*-butyl acetate (1:1) and phenol space velocity (LHSV = 1.1 h^{-1}) were used for all the catalytic runs. Product analysis shows that 4-*t*-butyl phenol (4-TBP), 2-*t*-butyl phenol (2-TBP) and 2,4-di-*t*-butyl phenol (2,4-DTBP) are the major products along with small amounts of undesired cracked and oligomerised products. The formation of the above products indicates that *t*-butylation occurs predominantly at carbon site in phenol. No O-alkylated product is observed over all the catalysts at all the temperatures studied.

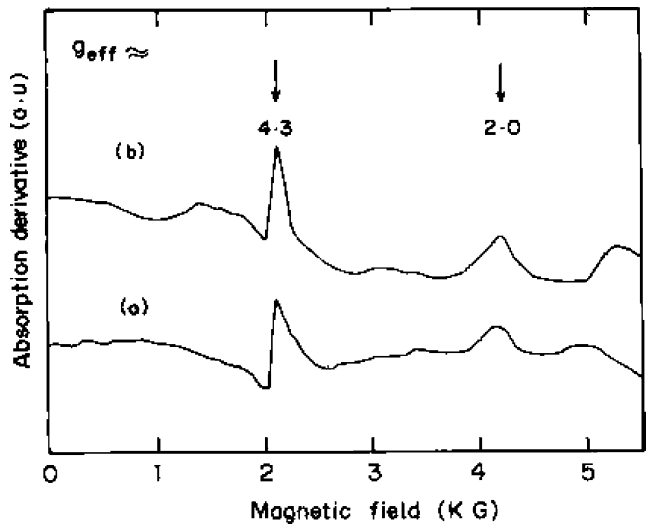

Fig. 6. EPR spectra of Fe–Al-MCM-41 catalysts (a) Fe–Al-MCM-41 (50) and (b) Fe–Al-MCM-41 (100).

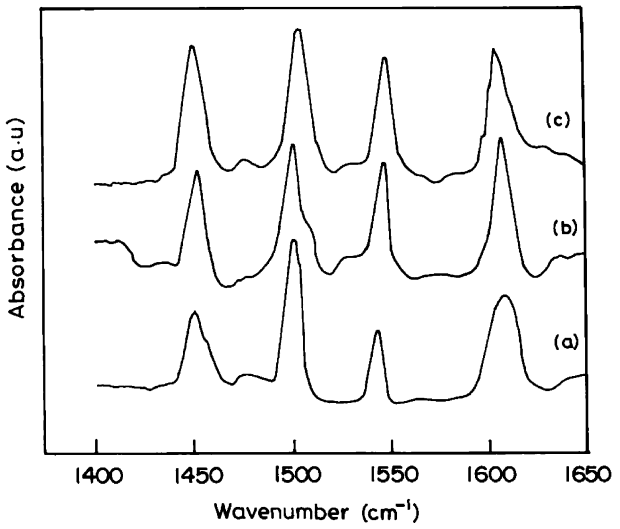

Fig. 7. FT-IR spectra of (a) Al-MCM-41 (50), (b) Zn–Al-MCM-41 (50) and (c) Fe–Al-MCM-41 (50) catalysts containing adsorbed pyridine.

3.2.1. Effect of feed ratio

In order to choose an optimum feed ratio, *t*-butylation of phenol was carried out at 300 °C over H-form of Al-MCM-41 (50), Zn– and Fe–Al-MCM-41 (50) catalysts by varying (2:1, 1:1, 1:2 and 1:3) molar feed ratios of phenol to *t*-butyl acetate (TBA). The catalytic runs were carried out at atmospheric pressure and at the phenol space velocity of 1.1 h^{-1}. The products distribution at various molar feed ratios is presented in Table 2. Fig. 8 shows that the phenol conversion and product selectivity at various feed ratios over Fe–Al-MCM-41 at 300 °C. It is observed that conversion increases by increasing TBA content (decreasing phenol content). When the phenol to TBA molar feed ratio

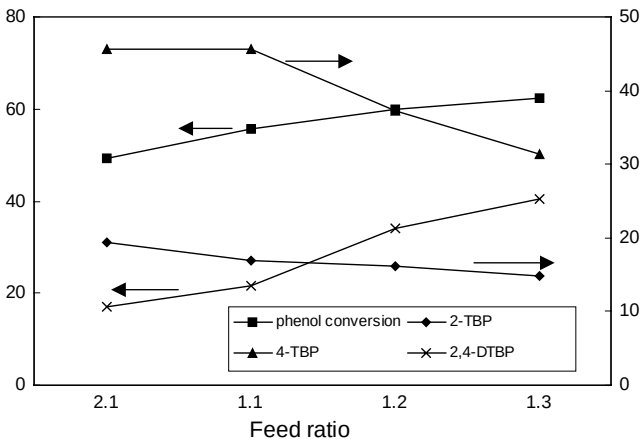

Fig. 8. Effect of feed ratio on phenol conversion and product selectivity over Fe–Al-MCM-41 (50).

Table 2
Effect of feed molar ratio and phenol space velocity on the product distribution over different catalysts at 300 °C

Feed ratio	Al-MCM-41 (50)					Zn–Al-MCM-41 (50)					Fe–Al-MCM-41 (50)				
	Conv.[a]	2-TBP	4-TBP	DTBP	Others	Conv.[a]	2-TBP	4-TBP	DTBP	Others	Conv.[a]	2-TBP	4-TBP	DIPP	Others
2:1	37.5	15.0	15.0	3.0	4.5	46.7	16.3	20.6	4.8	5.0	49.2	15.2	22.5	5.2	6.3
1:1	44.6	16.5	17.0	5.8	5.3	51.2	16.3	22.2	6.2	6.5	55.6	15.0	25.3	7.5	7.8
1:2	47.2	14.3	15.7	10.2	7.0	52.7	13.2	19.6	11.5	8.4	60.0	15.5	22.3	12.7	9.5
1:3	47.8	12.5	14.4	12.4	8.5	55.3	12.5	18.2	13.3	11.3	62.4	14.7	19.6	15.8	12.3
LHSV (h^{-1})															
0.55	47.2	18.0	19.0	6.7	4.5	55.2	17.5	23.6	8.6	5.5	60.3	15.8	27.5	11.0	6.0
1.1	44.6	16.5	17.0	5.8	5.3	51.2	16.3	22.2	6.2	6.5	55.6	15.0	25.3	7.5	7.8
1.65	36.2	13.2	13.0	4.7	5.3	40.4	12.0	16.3	3.8	8.3	46.3	12.2	20.5	4.2	9.4
2.2	29.2	10.3	9.5	3.4	6.0	32.7	9.0	12.2	3.0	8.5	37.5	9.0	16.2	2.5	9.8

Weight of catalyst: 1.0 g, time-on-stream = 1 h.
[a] Conversion (wt.%) based on phenol.

decreased from 2:1 to 1:3 the phenol conversion is found to increase from 37.5 to 47.8 wt.% over Al-MCM-41 (50). An abrupt increase in conversion is observed when changing the feed molar ratio from 2:1 to 1:1 and further change in feed ratio (1:2 and 1:3) leads to a marginal increase in phenol conversion over all the catalytic systems. Similarly the phenol conversion is found to increase from 46.7 to 55.3 and 49.2 to 62.4 wt.% over Zn– and Fe–Al-MCM-41 (50), respectively, at the above said feed ratios and temperature. The increase in phenol conversion with decreasing phenol-to-TBA ratio may be attributed to competition of polar molecule TBA with phenol for the adsorption sites, and with increasing molar excess of the alkylating agent, the phenol conversion increases similar to the previous reports [9,33]. The increase in conversion might be due to increased adsorption of TBA over the catalyst surface and more availability of *t*-butyl cations near the chemisorbed phenol. From Table 2 it can be clearly depicted that the selectivity to 4-TBP decreases with increasing TBA content in the feed. The extent of decrease in 4-TBP selectivity is marginal when changing the feed ratio from 2:1 to 1:1 and a drastic decrease is observed on changing it to 1:2 and 1:3 over all the catalytic systems. The selectivity to 4-TBP was fond to decrease from 40.0 to 30.1% over Al-MCM-41 (50) when the feed ratio changed from 2:1 to 1:3. The corresponding decrease in 4-TBP selectivity over Zn– and Fe–Al-MCM-41 (50) is 44.1–32.9 and 45.7–31.4%, respectively, thereby causing simultaneous increase in 2,4-DTBPs selectivity. At lower phenol to TBA feed ratios the selectivity to 4-TBP decreased and the undesired products selectivity increases. This implies that increase in TBA content would not prevent the adsorption of phenol. The 4-TBP yielded by adsorbed phenol also has sufficient opportunity to react at the *o*-position with other *t*-butyl cations distributed over the entire channel of the catalyst surface to yield 2,4-DTBP. The selectivity to 2,4-DTBP is found to increase from 8.0 to 25.9% over Al-MCM-41 (50) and 10.3 to 24.0 and 10.6 to 25.3% over Zn– and Fe–Al-MCM-41 (50), respectively. The extent of decrease in 4-TBP selectivity is small when the phenol to TBA ratio is decreased from 2:1 to 1:1 and further increase in TBA content leads to drastic decrease in 4-TBP selectivity. The increase in DTBPs selectivity with increasing TBA content may be due to higher concentration of TBA, which leads to polyalkylation. The selectivity to 2-TBP decreased from 40.0 to 26.2% when the feed ratio is changed from 2:1 to 1:3 over Al-MCM-41 (50). Depending on the phenol conversion and 4-TBP selectivity (principally aimed product) the molar feed ratio of 1:1 was chosen as the optimum for further studies.

3.2.2. Effect of phenol flow rate

The effect of phenol space velocity on phenol conversion and product selectivity was studied by carrying out the *t*-butylation of phenol at various (LHSV = 0.55, 1.1, 1.65 and 2.2 h^{-1}) phenol space velocities at 300 °C over H-form of Al-MCM-41 (50), Zn– and Fe–Al-MCM-41 (50) catalysts and the results are presented in Table 2. The optimised flow rate of 1:1 was followed. The phenol conversion was found to decrease from 47.2 to 29.2 wt.% when the phenol space velocity is increased from 0.55 to 2.2 h^{-1} over Al-MCM-41 (50) and the same was found to decrease from 55.2 and 60.3 to 32.7 and 37.5 wt.%, respectively, over Zn– and Fe–Al-MCM-41 (50) catalysts. A slight fall in phenol conversion is observed up to phenol space velocity LHSV = 1.1 h^{-1} and further increase leads to a drastic fall in phenol conversion over all the catalytic systems. The low phenol conversion at high space velocities could be accounted in terms of the shorter contact time, i.e. the less adsorption of TBA on the Brønsted acid sites, which could be attributed to the side reaction (oligomerisation) of TBA [4,20]. The 4-TBP selectivity is found to decrease with increasing phenol space velocity over all the catalytic systems. The decrease in 4-TBP selectivity is marginal up to the phenol space velocity of 1.1 h^{-1} and drastic thereafter. The selectivity to 4-TBP was found to be maximum (60.0%) over Fe–Al-MCM-41 than other catalysts at the phenol space velocity of 0.55 h^{-1}. The low selectivity to 4-TBP at lower space velocity 0.55 h^{-1} could be attributed to the dealkylation of butyl phenol to phenol and coke formation due to longer contact time [33]. The selectivity to 2,4-DTBP

is found to decrease with increasing phenol space velocity. The decrease in the 2,4-DTBP selectivity was found to be 14.2–11.6% over Al-MCM-41 (50), when the space velocity is increased from 0.55 to 2.2 h^{-1} this could be due to the fact that the increase in phenol space velocity may suppress the consecutive alkylation of 4-TBP to 2,4-DTBP as it is a time-dependent reaction. The increase in selectivity to 2-TBP with increase in space velocity might be due to an increase in the amount of phenol in the vapour phase, thus enhancing vapour phase reaction of phenol to *t*-butyl cation on the catalyst surface. Considering the phenol conversion as well as *p*-isomer selectivity, LHSV of 1.1 h^{-1} was chosen as the optimum phenol space velocity for further studies.

3.2.3. Effect of reaction temperature

The *t*-butylation of phenol was carried out over H-form of mesoporous Al-MCM-41 (Si/Al = 50 and 100), Zn–Al-MCM-41 (Si/Al = 50 and 100) and Fe–Al-MCM-41 (Si/Fe = 50 and 100) molecular sieves at 250–400 °C in steps of 50 °C. The optimised phenol to TBA molar ratio (1:2) and phenol space velocity (1.1 h^{-1}) were followed for all the catalytic runs. The phenol conversion at various reaction temperatures over all the above catalytic systems is presented in Fig. 9 and the product distribution in Table 3. The phenol conversion registers an increase from 250 to 350 °C and slight decrease at 400 °C over all the catalytic systems. The decrease in phenol conversion at higher temperature could be due to the simultaneous de-*t*-butylation of the formed product *t*-butyl phenol into phenol and lower hydrocarbons, and could be due to the blocking of acid sites by polybutenes and coke formation. At higher reaction temperatures the formation of undesired products were enhanced. The formed undesired products may consume the reactant (TBA) without producing products and might lead to lower phenol conversion. Zhang et al. [4] from their study of alkylation of phenol with *t*-butyl alcohol catalysed by zeolite Hβ has reported the similar results.

In mesoporous Al-MCM-41 molecular sieve catalysts, the increase in Al content and hence the total acidity is found to increase the phenol conversion at all the temperatures studied. Similar trend was observed over Zn– and Fe–Al-MCM-41 molecular sieves. At 350 °C the Al-MCM-41 with Si/Al ratio 100 and 50 show the phenol conversion of 43.7 and 47.0 wt.%, respectively. The phenol conversion over Zn and Fe incorporated Al-MCM-41 is found to be always higher than that of pure Al-MCM-41 catalysts at all the temperatures studied. The phenol conversion over Zn– and Fe–Al-MCM-41 with Si/M = 100 and 50 (M = Zn and Fe) are found to be 50.3 and 56.0 and 57.8 and 61.0 wt.%, respectively, at 350 °C. The enhanced effect in phenol conversion due to incorporation of Lewis acidic metals could be attributed to the strengthening of the

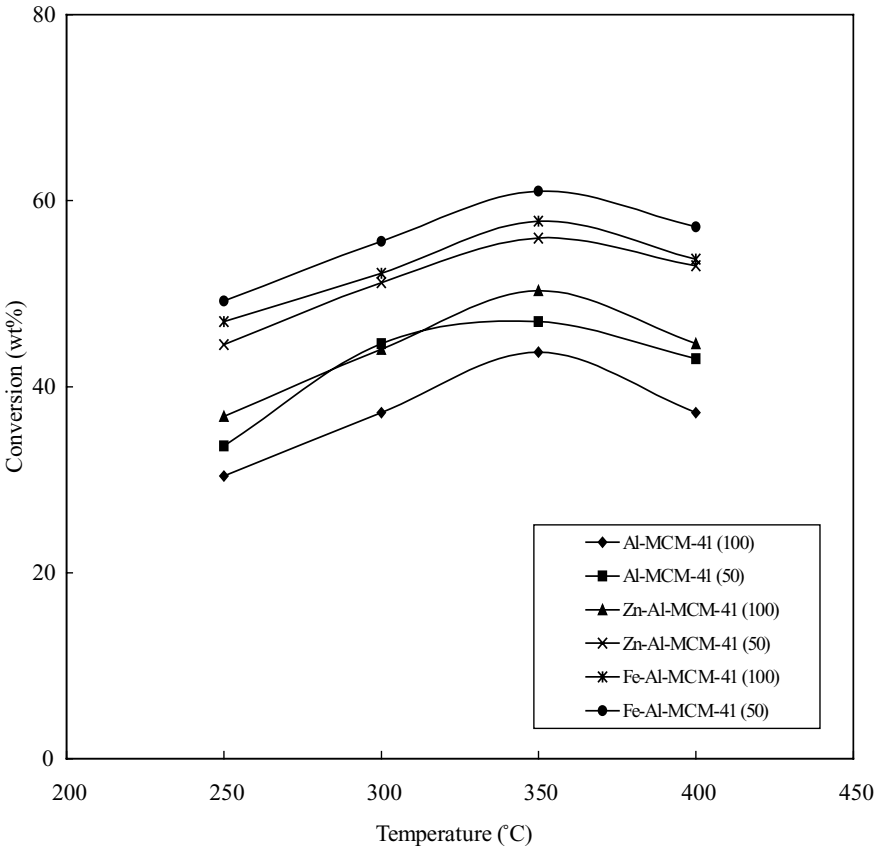

Fig. 9. Effect of temperature on phenol conversion over various catalysts.

Table 3
Products distribution of phenol *t*-butylation over different catalysts at different reaction temperatures

	250 °C						300 °C					
	1	2	3	4	5	6	1	2	3	4	5	6
2-TBP	14.0	14.5	15.0	16.6	16.0	15.0	14.8	16.5	15.0	16.3	15.0	15.0
4-TBP	7.8	10.2	12.2	16.3	18.5	20.5	12.4	17.0	18.0	22.2	23.2	25.3
2,4-DTBP	6.2	5.9	6.3	7.4	8.0	8.5	6.0	5.8	5.5	6.2	7.0	7.5
Others	2.5	3.0	3.3	4.2	4.5	5.2	4.0	5.3	5.5	6.5	7.0	7.8
Conversion[a]	30.4	33.6	36.8	44.5	47.0	49.2	37.2	44.6	44.0	51.2	52.2	55.6
	350 °C						400 °C					
	1	2	3	4	5	6	1	2	3	4	5	6
2-TBP	16.3	15.5	14.6	15.3	14.0	10.7	12.2	13.1	12.2	12.4	9.4	6.0
4-TBP	15.6	19.2	22.8	26.7	30.4	34.3	14.4	18.0	19.7	26.1	30.4	33.2
2,4-DTBP	6.5	5.5	5.5	5.5	5.8	6.0	4.0	4.5	3.7	3.0	4.3	3.3
Others	5.3	6.8	7.4	8.5	9.6	10.0	6.6	7.4	9.0	11.5	12.6	14.7
Conversion[a]	43.7	47.0	50.3	56.0	57.8	61.0	37.2	43.0	44.6	53.0	53.7	57.2

1, Al-MCM-41 (100); 2, Al-MCM-41 (50); 3, Zn–Al-MCM-41 (100); 4, Zn–Al-MCM-41 (50); 5, Fe–Al-MCM-41 (100); 6, Fe–Al-MCM-41 (50). Feed molar ratio = 1:2, phenol space velocity = 1.1 h^{-1}.

[a] Conversion (wt.%) based on phenol.

nearby Brønsted acid sites and it may enhance the activity of catalyst in phenol conversion.

In 4-TBP selectivity, if phenol is getting chemisorbed on the Brønsted acid sites, and also there is an unequal electron density distribution than the *m*-position, then the *p*-position alone can be brought into electrophilic attack with *t*-butyl cation to yield the product 4-TBP. Formation of 2-TBP is to be based on the reaction between phenol in the vapour phase and *t*-butyl cation on the catalyst surface. In line with this, the 2-TBP is also produced with less selectivity than 4-TBP. The selectivity to 2,4-DTBP, which is to be derived by consecutive alkylation of either 2-TBP or 4-TBP, is also less due to less concentration of *t*-butyl cation on the catalyst surface.

The comparison of product selectivities of Al-MCM-41, Zn– and Fe–Al-MCM-41 catalysts at a definite reaction conditions allow us to study the effect of Zn and Fe incorporation and hence the acidity of the catalysts on the product selectivity. Fig. 10 represents the selectivities of the individual products over Al-MCM-41 (50), Zn– and Fe–Al-MCM-41 (50) catalysts at 350 °C. It is observed that the selectivity of 4-TBP is found to be higher over

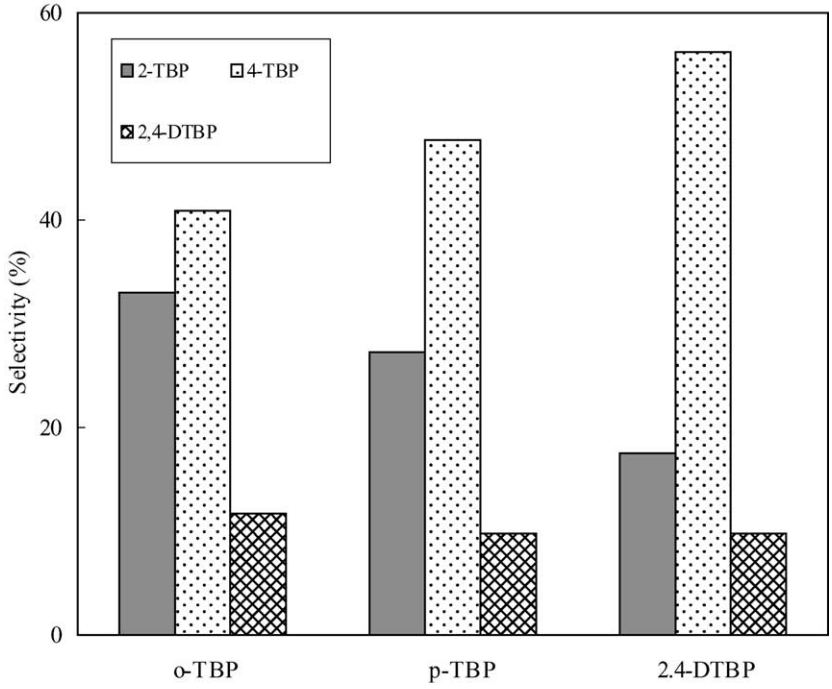

Fig. 10. Al-MCM-41 (50); Zn–Al-MCM-41 (50); Fe–Al-MCM-41 (50).

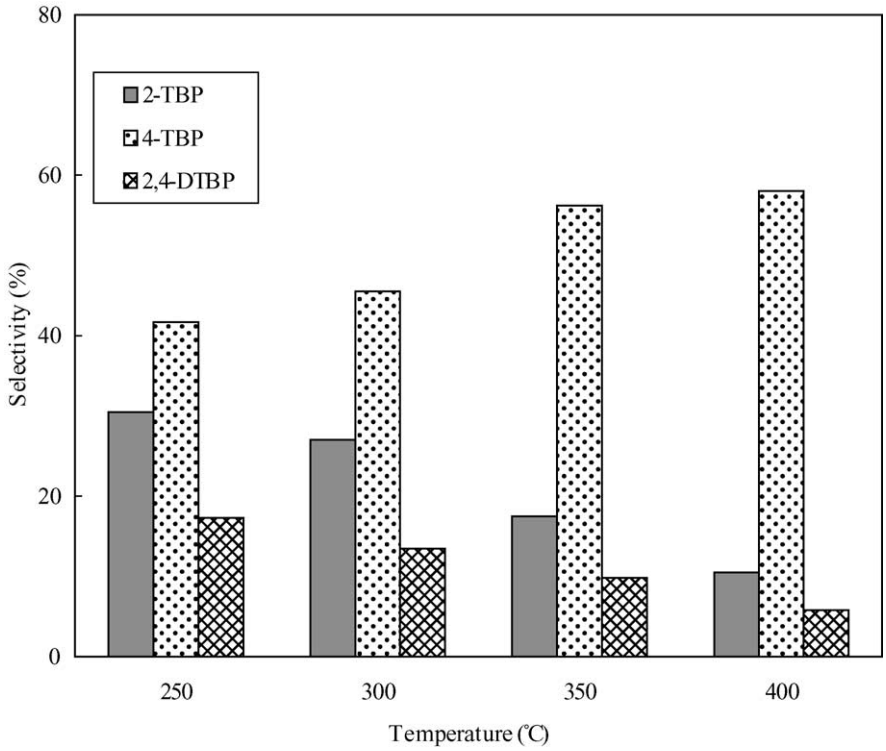

Fig. 11. Effect of temperature on the products selectivity over Fe–Al-MCM-41 (50) catalyst.

Zn– and Fe–Al-MCM-41 catalysts than that of Al–MCM-41 catalysts. Zn– and Fe–Al-MCM-41 (50) catalysts show the 4-TBP selectivity of 47.7 and 56.2%, respectively, which are significantly higher than that over Al-MCM-41 (50) (40.9%). The higher selectivity of 4-TBP over Zn and Fe incorporated catalysts can be accounted in terms of strong Brønsted acid sites strengthened by Lewis acid sites due to incorporation of Zn and Fe, and may favour the *p*-*t*-butylation. In contrast, the 2-TBP selectivity is found to decrease on Zn and Fe incorporation. Also, the selectivity to undesired products is found to be higher over Zn and Fe catalysts due to stronger acidity.

The effect of temperature on the selectivity of individual products in *t*-butylation of phenol over the best-performed catalyst Fe–Al-MCM-41 (50) is presented in Fig. 11. On increasing the temperature, the 4-TBP selectivity is found to increase steadily over all the catalytic system. The 2-TBP and 2,4-DTBP selectivities are found to decrease with increasing reaction temperature due to steric hindrance as well as thermodynamically unfavoured 2-TBP readily isomerised into less hindered, partially kinetically favourable 4-TBP. Between the Zn and Fe substituted catalysts, Fe–Al-MCM-41 (50) shows the higher selectivity towards 4-TBP and 2-TBP.

The presence of phenolic (–OH) group kinetically favours *o*-alkylation [20]. Tanabe and Nishizaki [34] and Klemm et al. [35] carried out phenol *t*-butylation and suggested a vertical orientation in the adsorption of phenol molecules at Lewis acid sites, the *o*-position of phenol being close to the surface and *t*-butylation at *o*-position occurred predominantly. But the Brønsted acid sites strongly interact with aromatic ring of the adsorbed phenol, thus bringing it closer to the surface and permitting *t*-butylation at *o*- and *p*-positions. Similarly in the present case, catalysts with strong Brønsted acid sites are found to enhance the *t*-butylation at *p*-position, i.e. Fe–Al-MCM-41 (50) shows the maximum *p*-isomer (4-TBP) selectivity among the catalysts studied may be due to strong Brønsted acid sites generated by the incorporation of Fe as evidenced by TPD of ammonia and pyridine adsorbed FT-IR spectroscopy studies. In the case of 2-TBP, due to steric hindrance by bulky *t*-butyl group in its *o*-position, most of the formed 2-TBPs are isomerised into 4-TBP on increasing the reaction temperature. Also, due to bulky nature of *t*-butyl group in *o*-position, the *o*-TBP (2-TBP) could react with TBA to form 2,4-DTBP. Among the catalysts studied, catalyst Fe–Al-MCM-41 (50) shows the maximum phenol conversion and 4-TBP selectivity at 350 °C.

In order to study the effect of Zn and Fe incorporation in Al-MCM-41 framework on catalytic activity, *t*-butylation of phenol was also carried out over Zn and Fe ion exchanged Al-MCM-41 (50) catalyst at optimised reaction conditions. Catalysts Zn/ and Fe/Al-MCM-41 (50) show the phenol conversion 44.0 and 50.2 wt.% with 35.4 and 41.3% of 4-TBP selectivity, respectively, which are considerably lower than that of Zn– and Fe–Al-MCM-41 (50) catalysts at 350 °C. The lower activity of Zn and Fe ion exchanged catalysts indicate that the Zn and Fe incorporated in the framework

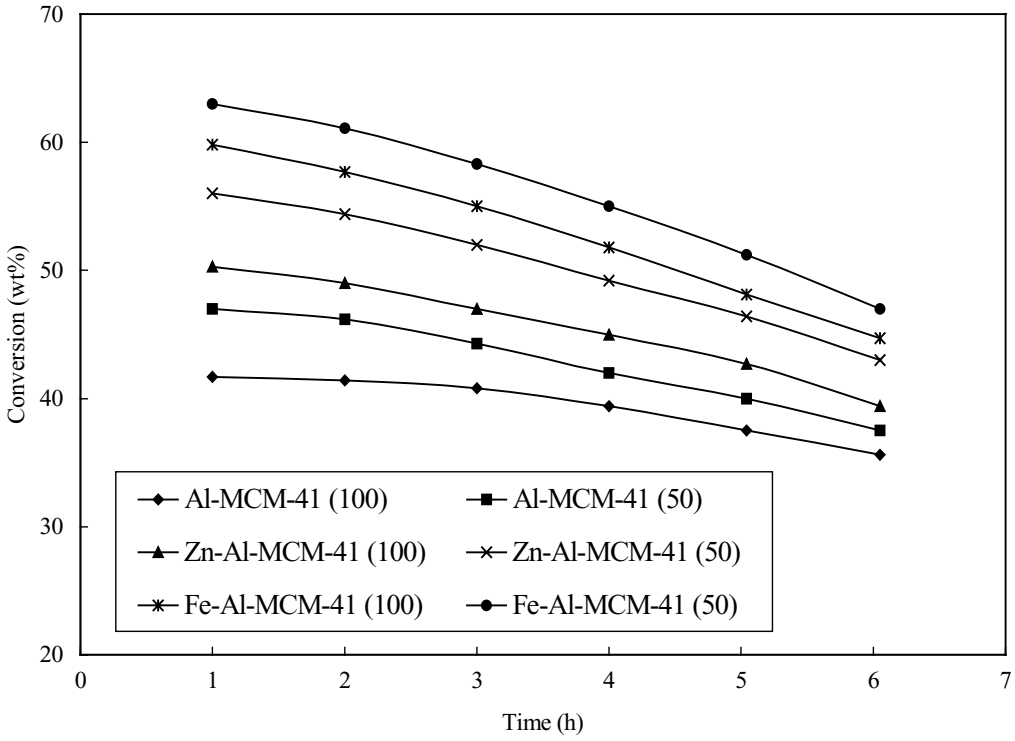

Fig. 12. Effect of time-on-stream on phenol conversion over the mesoporous molecular sieves at 350 °C.

only responsible for the enhanced activity, i.e. tetrahedrally coordinated Zn and Fe ions in Al-MCM-41 framework enhancing their catalytic activity.

4. Effect of time-on-stream

The effect of time-on-stream on conversion and products selectivity was studied at 350 °C with feed ratio 1:1 and LHSV 1.1 h^{-1} to understand the sustainability of the H-form of the above catalysts in *t*-butylation of phenol. Phenol conversion obtained over different catalysts during the time-on-stream study is presented in Fig. 12. It is found that all the catalysts loose their activity with time. The activity loss is small up to a period of 3 h and higher thereafter. Catalysts with strong acid sites deactivates faster than other catalysts. The faster deactivation may be due to higher cracking activity and enhanced coke formation by strong acid sites of the catalyst [36]. The major product 4-TBP exhibits uniform decrease in selectivity with stream. Conversely 2-TBP exhibits a reverse trend. The decrease in selectivity to 4-TBP is due to gradual blocking of active sites leading to prevention of chemisorption of phenol.

5. Conclusion

The low angle XRD analysis of hydrothermally synthesised Zn– and Fe–Al-MCM-41 catalysts reveal that the hexagonal structure of MCM-41 was retained after the incorporation of Zn and Fe in Al-MCM-41 framework. Further, the higher *d*-spacing values of Zn– and Fe–Al-MCM-41 catalysts than that of pure Al-MCM-41 confirms the insertion of Zn and Fe in Al-MCM-41 framework. The nitrogen adsorption studies indicate the mesoporous nature of the materials. The ^{27}Al MAS NMR studies confirm the tetrahedral co-ordination of aluminium. A band around 275 nm in DRS and two signals at $g = 2.0$ and 4.25 in EPR spectrum confirms the tetrahedral co-ordination of Fe in Fe–Al-MCM-41. The acidity measurements reveal that appropriately positioned Lewis acid sites generated by Zn and Fe incorporation strengthen the Brønsted acid sites. Vapour phase *t*-butylation of phenol with TBA over the above-characterised materials indicates that the phenol to TBA molar ratio of 1:1 and phenol space velocity LHSV = 1.1 h^{-1} were optimum for better phenol conversion and 4-TBP selectivity. Zn– and Fe–Al-MCM-41 catalysts always show higher phenol conversion than Al-MCM-41 due to stronger acidity generated by Zn and Fe incorporation. Also, it is found that the incorporation of Zn and Fe in tetrahedral co-ordination of Al-MCM-41 enhances the activity of the catalysts. The phenol conversion as well as 4-TBP selectivity is found to decrease with time-on-stream.

References

[1] A. Knop, L.A. Pilato, Phenolic Resins Chemistry, Springer, Berlin, 1985.

[2] J.F. Lorenc, G. Lambeth, W. Scheffer, in: M. Howe-Grant, J.I. Kroschwitz (Eds.), Kirk-Othmer Encyclopedia of Chemical Technology, vol. 2, Wiley, New York, 1992, p. 113.
[3] A. Corma, H. Garcia, J. Primo, J. Chem. Res. (s) 1 (1988) 40.
[4] K. Zhang, C. Huang, H. Zhang, S. Xiang, S. Liu, D. Xu, H. Li, Appl. Catal. A: Gen. 166 (1998) 89.
[5] JP 01,251,633.
[6] M. Inoue, S. Enomoto, Chem. Pharm. Bull. 24 (1976) 2199.
[7] S. Karuppannasamy, K. Narayanan, C.N. Pillai, J. Catal. 66 (1980) 281.
[8] R. Pierantozzi, A.F. Nordquist, Appl. Catal. 21 (1986) 263.
[9] R.F. Parton, J.M. Jacobs, H.V. Ootehem, P.A. Jacobs, Stud. Surf. Sci. Catal. 46 (1988) 211.
[10] A. Mitra, PhD Thesis, IIT Bombay, 1997, p. 55.
[11] C.T. Kresge, M.E. Leonowicz, W.J. Roth, J.C. Vartuli, J.S. Beck, Nature 359 (1992) 710.
[12] A. Corma, Chem. Rev. 97 (1997) 2373.
[13] K.S.N. Reddy, B.S. Rao, P.V. Shirakar, Appl. Catal. A 121 (1995) 191.
[14] R. Schmidt, D. Akporiaye, M. Stoecke, O.H. Ellestad, Stud. Surf. Sci. Catal. A 84 (1994) 61.
[15] M. Busio, J. Janchen, J.H.C. Van Hooff, Micropor. Mater. 5 (1995) 211.
[16] R. Ryoo, J.M. Kim, J. Chem. Soc., Chem. Commun. (1995) 711.
[17] T. Inui, J.B. Kim, M. Seno, Catal. Lett. 29 (1994) 271.
[18] O. Franke, J. Rathousky, G. Schultz-Ekloff, J. Starek, A. Zukkal, Stud. Surf. Sci. Catal. A 84 (1994) 77.
[19] K.A. Koyano, T. Tatsumi, J. Chem. Soc., Chem. Commun., (1996) 145.
[20] A. Sakthivel, S.K. Badamali, P. Selvam, Micropor. Mesopor. Mater. 39 (2000) 457.
[21] N. He, S. Bao, Q. Xu, Appl. Catal. A: Gen. 169 (1998) 29.
[22] R. Savidha, A. Pandurangan, Appl. Catal. A: Gen., in press.
[23] X.S. Zhao, G.Q. Lu, G.J. Millar, Catal. Lett. 38 (1996) 33.
[24] P.J. Branton, P.G. Hall, K.S.W. Sing, H. Reichert, F. Schuth, K. Unger, J. Chem. Soc., Faraday Trans. 90 (19) (1994) 2965.
[25] H.B.S. Chan, P.M. Budd, T.deV. Naylor, J. Mater. Chem. 11 (2001) 951.
[26] R. Mokaya, W. Jones, J. Catal. 172 (1997) 211.
[27] K. Chaudhari, T.K. Das, A.J. Chandwadkar, S. Sivasanker, J. Catal. 189 (1999) 81;
Y. Wang, Q. Zhang, T. Shishudo, K. Takehira, J. Catal. 209 (2002) 186.
[28] B. Echchahed, A. Moen, D. Nicholson, L. Bonneviot, Chem. Mater. 9 (1997) 1716.
[29] Y. Wang, Q. Zhang, T. Shishido, K. Takehira, J. Catal. 209 (2002) 186.
[30] D.G. Derovane, M. Mestsdagh, L. Vieluoge, J. Catal. 33 (1974) 169.
[31] S. Bordiga, R. Buzzoni, F. Geobaldo, C. Lamberti, E. Giametto, A. Zecchina, G. Petrini, G. Tozzola, G. Valaic, J. Catal. 158 (1996) 486.
[32] M.L. Poutsma, Zeolite chemistry and catalaysis, in: J.A. Rabo (Ed.), ACS Monograph, vol. 171, ACS, Washington, DC, 1976, p. 437.
[33] S. Subramanian, A. Mitra, C.V.V. Satyanarayana, D.K. Chakrabarty, Appl. Catal. A 159 (1997) 229.
[34] K. Tanabe, T. Nishizaki, in: F.C. Tompkins (Eds.), Proceedings of the Sixth International Congress on Catalysis, The Chemical Society, London, 1977.
[35] L.H. Klemm, C.E. Kloptenstein, J. Shabtar, J. Org. Chem. 35 (1970) 1069.
[36] E. Santaccesaria, D. Grasso, D. Gelosa, S. Carra, Appl. Catal. 64 (1990) 83.